

Optical harmonic generation in monolayer group-VI transition metal dichalcogenides

Anton Autere,¹ Henri Jussila,¹ Andrea Marini,² J. R. M. Saavedra,² Yunyun Dai,¹ Antti Säynätjoki,^{1,3} Lasse Karvonen,¹ He Yang,¹ Babak Amirsolaimani,⁴ Robert A. Norwood,⁴ Nasser Peyghambarian,^{4,5,1} Harri Lipsanen,¹ Khanh Kieu,⁴ Francisco Javier García de Abajo,^{2,6} and Zhipei Sun^{1,7}

¹*Department of Electronics and Nanoengineering,*

Aalto University, P.O.Box 13500, FI-00076 Aalto, Finland

²*ICFO-Institut de Ciències Fotòniques, The Barcelona Institute of Science and Technology, 08860 Castelldefels, Barcelona, Spain*

³*Institute of Photonics, University of Eastern Finland, Yliopistokatu 7, FI-80101 Joensuu, Finland*

⁴*College of Optical Sciences, University of Arizona,*

1630 E. University Boulevard, Tucson, Arizona 85721, USA

⁵*Institute of Photonics, University of Eastern Finland, Yliopistokatu 7, FI-80101 Joensuu, Finland*

⁶*ICREA-Institució Catalana de Recerca i Estudis Avançats,*

Passeig Lluís Companys 23, 08010 Barcelona, Spain

⁷*QTF Centre of Excellence, Department of Applied Physics, Aalto University, FI-00076 Aalto, Finland**

Monolayer transition metal dichalcogenides (TMDs) exhibit high nonlinear optical (NLO) susceptibilities. Experiments on MoS₂ have indeed discovered very large second-order ($\chi^{(2)}$) and third-order ($\chi^{(3)}$) optical susceptibilities. However, third harmonic generation of other layered TMDs has not been reported. Further, the reported $\chi^{(2)}$ and $\chi^{(3)}$ of MoS₂ vary by several orders of magnitude, and a reliable quantitative comparison of optical nonlinearities across different TMDs has remained elusive. Here, we demonstrate third harmonic generation in WSe₂, MoSe₂ and WS₂, and three-photon photoluminescence in TMDs for the first time. We also report the first experimental study of $\chi^{(2)}$ and $\chi^{(3)}$ of four common TMD materials (MoS₂, MoSe₂, WS₂ and WSe₂) by placing different TMD flakes in close proximity to each other on a common substrate, allowing their NLO properties to be accurately obtained from a single measurement. $\chi^{(2)}$ and $\chi^{(3)}$ of the four monolayer TMDs have been compared, indicating that they exhibit distinct NLO responses. We further present theoretical simulations of these susceptibilities in qualitative agreement with the measurements. Our results of comparatively studying the NLO responses of different two-dimensional layered materials allow us to select the best candidates for atomic-scale nonlinear photonic applications, such as frequency conversion and all-optical signal processing.

I. INTRODUCTION

Recent years have witnessed a growing interest in two-dimensional (2D) layered materials for various electronic and photonic applications¹. This includes graphene², and transition metal dichalcogenides (TMDs), especially molybdenum disulphide (MoS₂)^{3–5}. TMDs possess fascinating layer-dependent optical and electrical properties, such as their layer-dependent bandgap. For example, bulk (group-VI) TMDs are typically indirect bandgap semiconductors, while in single atomic layer their bandgap becomes direct in the ~ 1.55 eV to 1.9 eV range^{3,4,6}. This renders monolayer TMDs (ML-TMDs) an attractive material for various optoelectronic applications, such as light emitting devices, detectors and modulators^{5,7}. ML-TMDs consist of two hexagonal lattices of chalcogen atoms separated by a plane of metal atoms occupying trigonal prismatic sites between the chalcogens⁵. Owing to their crystal structure, TMDs with an odd number of layers are noncentrosymmetric, while TMDs in bulk or with any even number of layers are centrosymmetric⁸. The lack of inversion symmetry in ML-TMDs leads to substantial second-order nonlinear optical susceptibility $\chi^{(2)}$.

Nonlinear optical (NLO) processes in 2D materials are of great interest for various technological

applications^{9–14}, such as frequency conversion, all-optical signal processing, ultrafast pulse generation, and parametric sources of quantum photon states. Furthermore, integration of 2D materials with photonic integrated circuits offers exciting prospects for new applications. Already, it has been shown that the NLO responses of 2D materials can be enhanced with waveguides^{9,15} and photonic crystal structures^{9,10,16}. With the promising NLO properties of 2D materials, this could enable on-chip devices, such as nonlinear light sources for quantum photonics and metrology or nonlinear phase modulation devices^{9,17}. In addition, the fundamental properties (e.g. crystal orientation) of different 2D materials can be probed via nonlinear optical processes such as second-harmonic generation (SHG), which shows significant importance for nanomaterial characterization^{9,18–20}. Thus far, research on TMDs has been focused on their electronic and linear-optical properties, with only few studies reporting on NLO properties. Several groups have already reported the observation of SHG in mono- and trilayer MoS₂^{8,21–23}, as well as in MoSe₂²⁴, WS₂²⁵, and WSe₂²⁶. Additionally, third order optical nonlinearity, quantified through the third-order susceptibility $\chi^{(3)}$, has been recently observed in few-layer²⁷ and monolayer^{28–30} MoS₂.

The rapid advance of the field has led to the obser-

vation of high-harmonic generation (HHG) in ML MoS₂ under intense laser excitation³¹. However, there are several aspects of the NLO response of TMDs that remain unexplored. For example, nonlinear optics with other TMDs (e.g., Third harmonic generation (THG) in WSe₂, MoSe₂ and WS₂) has not been fully studied⁹. Further, there is a large deviation in reported experimental values of $\chi^{(2)}$ for 2D materials (including TMDs), which could be partially attributed to differences between measurement conditions (e.g., excitation conditions, sample doping and strain effects) in those studies and also to the different substrates used in the measurements (e.g., different thicknesses and compositions). In fact, especially in the case of 2D materials, the substrate has a significant impact on harmonic generation^{32–34}, which makes the comparison of $\chi^{(2)}$ and $\chi^{(3)}$ values from different measurements problematic. For example in MoS₂, the reported values of $|\chi^{(2)}|$ at 800 nm excitation vary from 10^{-7} to 10^{-10} m V⁻¹ (i.e., by three orders of magnitude)^{8,21,22}. Furthermore, different experimental methods, such as two-wave mixing³⁵, multiphoton microscopy^{18,28,29}, and spatial self-phase modulation^{17,36} have been used to quantify the nonlinear susceptibilities of different materials, thus making the comparison even more involved. In conclusion, despite the importance of accurately assessing the NLO susceptibilities of TMDs and shedding light into their dependence on environmental conditions (e.g., as a tool to modulate the response at will), experimental studies so far available are fragmented and do not allow us to establish a systematic comparison between different materials.

Here, we present the first experimental study of the second- and third-order NLO properties of group-VI TMDs that is immune to differences in sample and excitation conditions. Monolayers of the four TMD materials, MoS₂, MoSe₂, WS₂ and WSe₂, are mechanically exfoliated and transferred onto a substrate, in close proximity to each other using a state-of-the-art dry-transfer technique. The effective NLO susceptibilities are then simultaneously determined for all four materials from a single set of SHG and THG images. As a result, the effective bulk-like second- and third-order nonlinear susceptibilities of all four materials are directly comparable. The excitation light source in our experiments is a mode-locked erbium-doped fiber laser with 1560 nm center wavelength. Thus, the resulting SHG and THG signals are in the visible-to-near-infrared range. Additionally, this provides information about $\chi^{(2)}$ and $\chi^{(3)}$ at 1560 nm, which is important for telecommunication applications. Moreover, the NLO responses of all four TMDs under consideration are examined with linear and elliptical polarization in this work. In addition, we theoretically calculate their second- and third-order nonlinear susceptibilities through a perturbative expansion of the two-band $\mathbf{k} \cdot \mathbf{p}$ Hamiltonian for such media, including the effect of the exciton resonance. Theoretical results are in qualitative agreement with measurements.

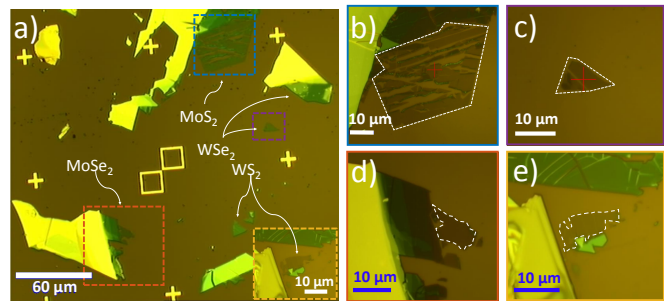


FIG. 1. (a) Optical image of four different TMDs positioned close to each other. Zoomed optical images of areas marked in (a) with colored rectangles for (b) MoS₂, (c) WSe₂, (d) MoSe₂ and (e) WS₂. White dashed contours in (b-e) indicate the monolayer areas.

II. EXPERIMENTAL STUDY

In our experiments, micromechanically exfoliated samples of MoS₂, MoSe₂, WS₂ and WSe₂ were transferred onto a Si/SiO₂ (285 nm) substrate, close to each other. The sample fabrication process is similar to that reported in Refs.^{37,38} (fabrication details in the Supplemental Material (SM)³⁹). The transferred flakes were then identified and characterized through optical contrast, Raman spectroscopy and photoluminescence (PL) measurements. The Raman peak separation can be used to extract the layer thickness^{40,41}. Details of these measurements are provided in the SM³⁹. Figure 1 shows an optical image of the fabricated sample. The ML flake of WS₂ is shown as an inset because it is placed slightly further away from the other materials, outside the image field of view. Additionally, graphene monolayers were exfoliated on a similar substrate for comparison. Strain and doping can have a significant effect on the (nonlinear) optical properties of 2D materials. The possible presence of strain is excluded based on the measured Raman spectra. For example, in Ref.⁴², it was shown that the E_{2g} peak in MoS₂ shifts by 4.5 cm⁻¹ per % strain and splits into two separate sub-peaks already at 0.5% strain, which we do not see in any of our measurements (see Figs. 2 and 3 in SM). Furthermore, the 2D materials are obtained from undoped bulk crystals and, since we are using a dry-transfer technique, the samples are not chemically doped. This is different from other transfer methods, in which the chemicals used during the transfer process might introduce the doping effect. The doping level can also be modified due to the substrate. For example, SiO₂ can have a high degree of charge impurities at the surface which can lead to altered doping level of the sample⁴³. The effect of doping on the nonlinear optical response of 2D materials is still largely unexplored. However, in Ref.³³ SHG from MoS₂ on SiO₂ and polymer substrates was measured. With a fundamental wavelength at 1600 nm they measured a $\chi^{(2)}$ of 6.3 pm/V on the SiO₂ substrate and 7 pm/V on the polymer substrate, suggesting that the doping from the substrate may not be substan-

tial. As noted earlier, to best of our knowledge, there are no studies on the effect of chemical or substrate induced doping on nonlinear optical properties of 2D materials at different wavelengths, so it is not possible to accurately assess the different contributions on the nonlinear optical responses of the four TMDs studied here. However, this is a highly interesting topic for future research.

The SHG and THG for the four materials under examination (Figure 2) were collected using a mode-locked fiber laser with 1560 nm center wavelength. Each different area (located within a distance of $< 150 \mu\text{m}$ from each other) possesses exfoliated TMD flakes, whose thicknesses range from one to a few atomic monolayers (see SM for thickness determination). The small distance between the locations of the exfoliated MoS_2 , MoSe_2 , WS_2 and WSe_2 allows us to easily compare the optical nonlinearities of the different materials. As a result, this excludes the effect of substrate and varying measurement conditions on the measured susceptibilities because the recorded SHG and THG powers can be obtained from the same SHG or THG image for all materials. The locations of the nonlinear microscopy images are indicated by dashed rectangles in the optical image in Fig. 1. We observed a SHG signal and a strong THG signal from all four TMDs, within a single image, of which Fig.2 selects zoomed regions.

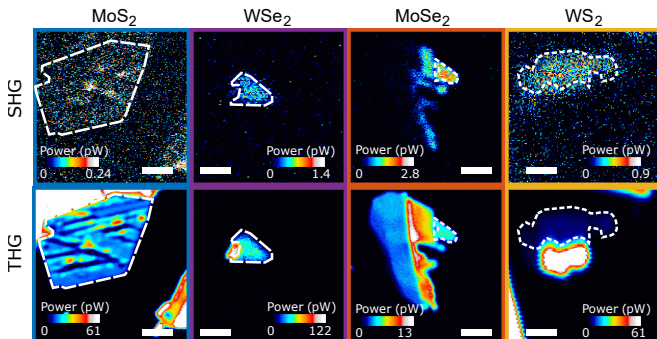


FIG. 2. SHG (top) and THG (bottom) images from the areas marked with colored dashed rectangles in the optical image of Fig. 1(a). Blue: MoS_2 . Purple: WSe_2 . Orange: MoSe_2 . Yellow: WS_2 . The scale bar for MoS_2 , WSe_2 and MoSe_2 is $10 \mu\text{m}$, for WS_2 is $5 \mu\text{m}$.

The reported values of SHG and THG signals are all obtained from the locations in which each TMD flake is single-layer thick. Prior to comparison, however, in order to prove that the measured signals at 780 nm and 520 nm in fact originate from SHG and THG, respectively, power dependent nonlinear microscopy measurements were performed for all four materials (see SM, Fig. S10). These measurements clearly indicate P^2 (SHG) and P^3 (THG) dependences, with the incident light power P . Note that this is the first time that THG can be observed in WSe_2 , MoSe_2 and WS_2 . The average powers of SHG and THG from monolayers of all four materials are shown in Fig. 3(a) and (b). Normally at a reasonable pump power, THG intensity is expected to be lower than SHG inten-

sity, due to the weaker intrinsic response of the higher-order nonlinear processes⁴⁴. It is surprising that THG is clearly stronger than SHG in all four TMDs at such a low average pump power (e.g. Fig. 3). The same effect was recently observed in MoS_2 , and explained with the contribution of trigonal warping to the second-order response²⁸. With low incident photon energies (0.8 eV here and in Ref. 28), SHG is weaker than expected for MoS_2 due to near-isotropic bands contributing to the SHG signal. Only trigonal warping breaks the approximate rotational invariance of the monolayer MoS_2 band structure, causing the SHG²⁸. More insight into the possible effects of trigonal warping or other causes (e.g. excitons) leading to the large observed ratio between THG and SHG, could be obtained by measuring the SHG and THG from all four materials with a large range of excitation wavelengths. Note that the SHG intensity from MoSe_2 is lower than the intensity of THG, even though the SHG is on resonance with the A exciton^{17,21,24,45,46}. Furthermore, we observe clearly distinct THG and SHG signals for different TMDs. For instance, THG is the largest from MoS_2 and the smallest from WSe_2 . In contrast, SHG from MoSe_2 is ~ 4 – 40 times larger than that from the other materials. This can be attributed to resonant enhancement in MoSe_2 because the energy of the A exciton in this material (~ 1.57 eV, 790 nm ⁴⁷) matches well with the wavelength (780 nm , 1.59 eV). In fact, the spectral overlap of excitonic PL and SHG is well visualized in Fig. 3 (c), which shows the PL spectrum measured with 532 nm excitation, and the multiphoton (MP) excited spectrum (containing SHG, THG and two-photon excited luminescence (2PL)) for MoSe_2 .

We note that the MP excited spectrum of WS_2 also shows a peak at $\sim 615 \text{ nm}$ (2.01 eV), corresponding to the location of the PL peak (Fig. 3d). Thus, we attribute this peak to three-photon excited luminescence (3PL) from monolayer WS_2 . Since 3PL ensues from a fifth-order NLO process⁴⁸, the probability of 3PL occurrence is very low. Interestingly, the intensity of 3PL is in the same range as the intensity of SHG. 2PL spectroscopy has been used to study the excitons in TMD monolayers because with 2PL it is possible to probe dark excitons states, that are forbidden by selection rules for one-photon excitation^{49,50}. Graphene and MoS_2 quantum dots have been used as 2PL probes in cellular and deep-tissue imaging^{51,52}. However, 3PL can provide better spatial resolution⁵³ and enable alternative excitation wavelengths, thus WS_2 might find new applications in biomedical imaging. Furthermore, 3PL spectroscopy might provide an alternative method for probing excitonic features in monolayer TMDs.

We estimate the effective second- and third-order nonlinear susceptibilities $|\chi_{\text{eff}}^{(2)}|$ and $|\chi_{\text{eff}}^{(3)}|$ of all TMDs from the measured average SHG and THG powers. The sheet susceptibility values, $\chi_s^{(n)}$, are estimated with the methods described in Ref. 29, by fitting the measured average

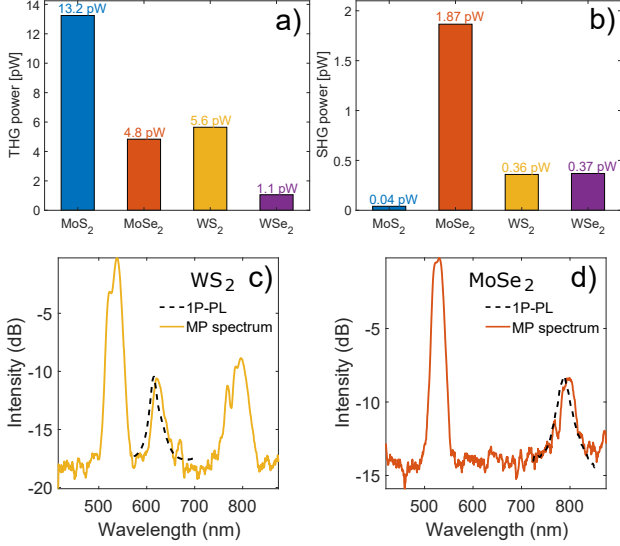


FIG. 3. Measured average powers of THG (a) and SHG (b) from monolayers of all four materials with 20 mW pump power (~ 2.7 kW peak power). Comparison between one-photon and multiphoton excited spectrum of (c) WS_2 and (d) MoSe_2 . Note that the intensities of one-photon and multiphoton spectra in (c) and (d) are not to scale.

powers to two equations

$$P_{\text{SHG}} = \frac{16\sqrt{2}S|\chi_s^{(2)}|^2\omega^2}{c^3\varepsilon_0 f\pi r^2\tau(1+n_2)^6} P_1^2, \quad (1)$$

$$P_{\text{THG}} = \frac{64\sqrt{3}S^2|\chi_s^{(3)}|^2\omega^2}{c^4\varepsilon_0^2(f\pi r^2\tau)^2(1+n_2)^8} P_1^3, \quad (2)$$

where $S = 0.94$ is the shape factor for Gaussian pulses, τ is the temporal pulse width, P_1 is the incident average power of the pump beam, f is the repetition rate, n_2 is the refractive index of the substrate at the pump wavelength, and ω is the angular frequency of the pump. The effective bulk-like second-order susceptibility of TMDs is obtained from the sheet susceptibilities as

$$|\chi_{\text{eff}}^{(n)}| = \frac{|\chi_s^{(n)}|}{t},$$

where t is the thickness of the TMD monolayer, 0.65 nm.

The $|\chi_{\text{eff}}^{(2)}|$ and $|\chi_{\text{eff}}^{(3)}|$ values measured from different TMDs in this work are presented in Table 1. Furthermore, $|\chi_{\text{eff}}^{(2)}|$ and $|\chi_{\text{eff}}^{(3)}|$ values for various monolayer TMDs from other measurements reported in the literature are presented in Table 1 in the SM.

Note that $|\chi_{\text{eff}}^{(2)}|$ values obtained in this work lie in the range between $5.4\text{--}37.0 \times 10^{-12} \text{ mV}^{-1}$ for all ML-TMDs. These values are in good agreement with those reported in the literature for TMDs when they have been measured with excitation wavelength in the IR region. For instance, the literature values of $|\chi_{\text{eff}}^{(2)}|$ for MoS_2 ^{28,29,54,55}

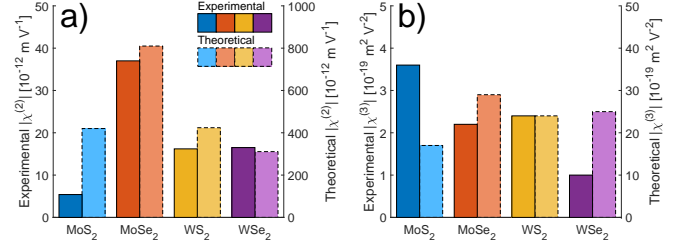


FIG. 4. Comparison of experimental and theoretical (a) $|\chi^{(2)}|$ and (b) $|\chi^{(3)}|$ of four TMDs at 1550 nm excitation.

ranges between 2.2×10^{-12} and $29 \times 10^{-12} \text{ mV}^{-1}$ and thus match reasonably well with the value of $5.4 \times 10^{-12} \text{ mV}^{-1}$ obtained in this work for 1560 nm excitation.

We note that the $|\chi_{\text{eff}}^{(2)}|$ for MoS_2 is two orders of magnitude smaller than what has been measured with 800 nm excitation^{8,21}. On the other hand, $|\chi_{\text{eff}}^{(3)}|$ values for all characterized TMDs are in the range between $1.0 \times 10^{-19} \text{ m}^2\text{V}^{-2}$ – $3.6 \times 10^{-19} \text{ m}^2\text{V}^{-2}$. We also find excellent agreement with previous literature values for $|\chi_{\text{eff}}^{(3)}|$ when measured at a similar wavelength. For instance, the magnitude of the $|\chi_{\text{eff}}^{(3)}|$ values for MoS_2 is of the order of $10^{-19} \text{ m}^2\text{V}^{-2}$ (see Refs.^{27–29}) and therefore in the same range as the value of $3.6 \times 10^{-19} \text{ m}^2\text{V}^{-2}$ reported in this work. The effect of the substrate should also be taken into account when comparing the values. In Ref. 29 the bulk-like $|\chi^{(2)}|$ and $|\chi^{(3)}|$ of MoS_2 were measured on glass and on Si/SiO_2 substrates. It was found that the $|\chi^{(2)}|$ did not exhibit significant change but the $|\chi^{(3)}|$ was enhanced by a factor of 5 due to the interferometric effect caused by the multilayer structure. However, this does not affect the comparison between the four materials, as the effect is the same for all of them, in this experiment.

The intensities of SHG and THG depend strongly on the polarization state of the pump and the crystallographic orientation of the sample^{8,28,29,31}. In order to explore this effect, we have measured SHG and THG from all four materials using elliptically polarized excitation light with varying degree of ellipticity. Figure 5(a–h) shows the measured SHG and THG intensities as a function of incident light polarization state. As shown in Fig. 5, the THG signal is strongest for linearly polarized excitation light and the smallest for circular polarization. In contrast, the SHG signal is the strongest for circularly polarized excitation light and the smallest for linearly polarized excitation light. Because all four materials belong to the point group D_{3h}^1 , similar results are obtained for the other crystals, MoSe_2 , WS_2 and WSe_2 . This paves the way for tailoring the nonlinear optical properties of 2D materials with heterostructures.

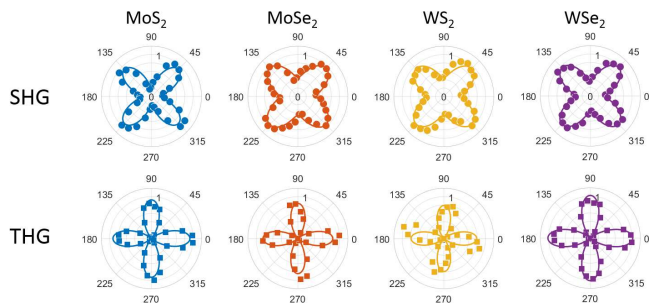


FIG. 5. Polar plots of normalized SHG and THG signals as a function of the quarter-wave plate (QWP) angle. The angle is defined between the polarization of the incident laser and the fast axis of the QWP.

III. THEORETICAL ANALYSIS AND COMPARISON TO EXPERIMENTAL VALUES

In order to obtain further insight into the origin of the NLO behavior under study, we theoretically calculate the second- and third-order nonlinear susceptibilities of all four materials through a perturbative expansion of the two-band $\mathbf{k} \cdot \mathbf{p}$ Hamiltonian for such media⁵⁶ under the minimum coupling prescription $\boldsymbol{\pi} = \mathbf{p} + e\mathbf{A}(t)$, where e is the electron charge, $\mathbf{A}(t)$ is the potential vector of the impinging light beam, and \mathbf{p} and $\boldsymbol{\pi}$ are the electron momentum and quasi-momentum, respectively. The two-

TABLE I. Theoretical and experimental $|\chi^{(2)}|$ and $|\chi^{(3)}|$ values of different TMD materials.

Material	$ \chi^{(2)} $ [$10^{-12} \frac{\text{m}}{\text{V}}$]		$ \chi^{(3)} $ [$10^{-19} \frac{\text{m}^2}{\text{V}^2}$]	
	Theor.	Exp.	Theor.	Exp.
MoS ₂	420	5.4	17	3.6
MoSe ₂	810	37.0	29	2.2
WS ₂	424	16.2	24	2.4
WSe ₂	311	16.5	25	1.0

band $\mathbf{k} \cdot \mathbf{p}$ Hamiltonian is obtained by fitting the valence and conduction bands of the tight-binding Hamiltonian reported in the literature⁵⁶ that account for both non-degenerate valleys and spin-orbit coupling. The effect of the exciton resonance on the nonlinear parameters of MoSe₂ is taken into account by introducing an effective exciton energy level in the single-particle Hamiltonian after fitting the linear conductivity with fully numerical Bethe-Salpeter calculations⁵⁷. Results are presented in Table I and compared with experiment in Figure 4, while technical details of the calculations are provided in the SM³⁹. These theoretical calculations predict a generally higher value of the nonlinear coefficients, roughly one order of magnitude larger than the corresponding measured quantities. Such calculations confirm that MoSe₂ is the ML TMD with highest $|\chi^{(2)}|$ nonlinear coefficient, although the relative difference with respect to other TMDs is not as marked as in experiments. A mismatch of rela-

tive values across different materials also appears in the $\chi^{(3)}$ calculations, which predict that MoSe₂ has the highest $|\chi^{(3)}|$, in contrast to experiment, in which MoS₂ exhibits the highest third-order nonlinearity. We envisage that this may be due to the effect of the substrate on electron many-body dynamics, which deserves further attention. In addition, the substrate is expected to induce subtle modifications on the band structure. While the linear response of the 2D layers under consideration remains unaffected because it mainly depends on the energy bandgap, the NLO response originates in the anharmonicity of the bands and thus it is much more sensitive to small modifications in the band structure arising from the interaction of ML-TMDs with the substrate. The comparison in our experimental results gives an indication of the trends when comparing different materials and also on the orders of the magnitude of the effects. Nevertheless, future theoretical efforts beyond the scope of this work are required to obtain a good quantitative agreement. We envisage that, in order to improve predictions, future theoretical efforts should lie in the inclusion of more bands, in the accounting for the interaction of the considered two-dimensional media with the substrate (which modifies the electronic band structure), and ultimately by performing first-principles calculations able to fully describe the nonlinear exciton dynamics beyond the effective exciton band model used in our calculations (see SM).

IV. CONCLUSIONS

In summary, we demonstrated third harmonic generation in WSe₂, MoSe₂ and WS₂, and three-photon photoluminescence in TMDs for the first time. We also reported the first direct comparison of second- and third-order optical nonlinearities in MoS₂, MoSe₂, WS₂ and WSe₂. The $\chi^{(2)}$ of MoSe₂ is found to be $\simeq 2$ -6 times larger than that of the other TMDs examined here. We attribute this effect to resonant enhancement of SHG in MoSe₂. The third-order nonlinear susceptibility $\chi^{(3)}$ of all four materials was found to be comparable to that of graphene, with the largest value $|\chi_{\text{eff}}^{(3)}| = 3.6 \times 10^{-19} \text{m}^2 \text{V}^{-2}$ observed for MoS₂. We obtain further insight into the NLO properties by theoretically calculating the second- and third-order nonlinear susceptibilities of all four materials, in qualitative agreement with measurements.

Furthermore, the effect of the degree of elliptical polarization of the incident light on the SHG and THG signals was examined and we found that the SHG signal was enhanced and the THG one was completely suppressed with circular polarization. Experimental results fit very well with expected values based on previously reported expressions derived from the crystal symmetry for MoS₂. The results presented here provide valuable information about the nonlinear properties of the different TMDs for the design of devices based on 2D materials and their

heterostructures in a wide range of applications, such as on-chip light sources and all-optical signal processing.

ACKNOWLEDGMENTS

We acknowledge funding from the Academy of Finland (276376, 284548, 295777, 298297 and 304666), TEKES

(NP-Nano, OPEC), the Nokia Foundation, Tekniikan edistämissäätiö (TES), the China Scholarship Council, Spanish MINECO (MAT2014-59096-P and SEV2015-0522), the European Commission (REA grant agreement No. 631610, Graphene Flagship 696656) and AGAUR (FLB-00492-2015 and 2014-SGR- 1400). We acknowledge the provision of facilities and technical support by Aalto University at Micronova Nanofabrication Centre.

-
- * zhipei.sun@aalto.fi
- ¹ A. C. Ferrari, F. Bonaccorso, V. Fal'ko, K. S. Novoselov, S. Roche, P. Boggild, S. Borini, F. H. Koppens, V. Palermo, N. Pugno, J. A. Garrido, R. Sordan, A. Bianco, L. Ballerini, M. Prato, E. Lidorikis, J. Kivioja, C. Marinelli, T. Ryhanen, A. Morpurgo, J. N. Coleman, V. Nicolosi, L. Colombo, A. Fert, M. Garcia-Hernandez, A. Bachtold, G. F. Schneider, F. Guinea, C. Dekker, M. Barbone, Z. Sun, C. Galiotis, A. N. Grigorenko, G. Konstantatos, A. Kis, M. Katsnelson, L. Vandersypen, A. Loiseau, V. Morandi, D. Neumaier, E. Treossi, V. Pellegrini, M. Polini, A. Tredicucci, G. M. Williams, B. H. Hong, J. H. Ahn, J. M. Kim, H. Zirath, B. J. van Wees, H. van der Zant, L. Occhipinti, A. Di Matteo, I. A. Kinloch, T. Seyller, E. Quesnel, X. Feng, K. Teo, N. Rupesinghe, P. Hakonen, S. R. Neil, Q. Tannock, T. Lofwander, and J. Kinaret, *Nanoscale* **7**, 4598 (2015).
 - ² F. Bonaccorso, Z. Sun, T. Hasan, and A. C. Ferrari, *Nat. Photonics* **4**, 611 (2010).
 - ³ K. F. Mak, C. Lee, J. Hone, J. Shan, and T. F. Heinz, *Phys. Rev. Lett.* **105**, 136805 (2010).
 - ⁴ A. Splendiani, L. Sun, Y. Zhang, T. Li, J. Kim, C.-Y. Chim, G. Galli, and F. Wang, *Nano Lett.* **10**, 1271 (2010).
 - ⁵ Q. H. Wang, K. Kalantar-Zadeh, A. Kis, J. N. Coleman, and M. S. Strano, *Nat. Nanotech.* **7**, 699 (2012).
 - ⁶ W. Jin, P.-C. Yeh, N. Zaki, D. Zhang, J. T. Sadowski, A. Al-Mahboob, A. M. van Der Zande, D. A. Chenet, J. I. Dadap, I. P. Herman, *et al.*, *Phys. Rev. Lett.* **111**, 106801 (2013).
 - ⁷ Z. Sun, A. Martinez, and F. Wang, *Nat. Photonics* **10**, 227 (2016).
 - ⁸ Y. Li, Y. Rao, K. F. Mak, Y. You, S. Wang, C. R. Dean, and T. F. Heinz, *Nano Lett.* **13**, 3329 (2013).
 - ⁹ A. Autere, H. Jussila, Y. Dai, Y. Wang, H. Lipsanen, and Z. Sun, *Adv. Mater.*, 1705963 (2018).
 - ¹⁰ T. Gu, N. Petrone, J. F. McMillan, A. van der Zander, M. Yu, G. Q. Lo, D. L. Kwong, J. Hone, and C. W. Wong, *Nat. Photonics* **6**, 554 (2012).
 - ¹¹ E. Hendry, P. J. Hale, J. Moger, and A. K. Savchenko, *Phys. Rev. Lett.* **105**, 097401 (2010).
 - ¹² S. Li, Y.-C. Lin, W. Zhao, J. Wu, Z. Wang, Z. Hu, Y. Shen, D.-M. Tang, J. Wang, Q. Zhang, H. Zhu, L. Chu, W. Zhao, C. Liu, Z. Sun, T. Taniguchi, M. Osada, W. Chen, Q.-H. Xu, A. T. S. Wee, K. Suenaga, F. Ding, and G. Eda, *Nat. Mater.* **17**, 535-542 (2018).
 - ¹³ X. Yang, Z. Sun, T. Low, H. Hu, X. Guo, F. J. García de Abajo, P. Avouris, and Q. Dai, *Adv. Mater.* **30**, 1704896 (2018).
 - ¹⁴ Z. Sun, *Nat. Photonics* **12**, 378-385 (2018).
 - ¹⁵ H. Chen, V. Corboliou, A. S. Solntsev, D.-Y. Choi, M. A. Vincenti, D. de Ceglia, C. de Angelis, Y. Lu, and D. N. Neshev, *Light Sci. Appl.* **6**, e17060 (2017).
 - ¹⁶ T. K. Fryett, K. L. Seyler, J. Zheng, C.-H. Liu, X. Xu, and A. Majumdar, *2D Mater.* **4**, 015031 (2017).
 - ¹⁷ G. Wang, S. Zhang, X. Zhang, L. Zhang, Y. Cheng, D. Fox, H. Zhang, J. N. Coleman, W. J. Blau, and J. Wang, *Photonics Res.* **3**, A51 (2015).
 - ¹⁸ A. Autere, C. Ryder, A. Saynatjoki, L. Karvonen, B. Amir-solaimani, R. Norwood, N. Peyghambarian, K. Kieu, H. Lipsanen, M. Hersam, and Z. Sun, *J. Phys. Chem. Lett.* **8**, 1343 (2017).
 - ¹⁹ J. Liang, J. Zhang, Z. Li, H. Hong, J. Wang, Z. Zhang, X. Zhou, R. Qiao, J. Xu, P. Gao, Z. Liu, Z. Liu, Z. Sun, S. Meng, K. Liu, and D. Yu, *Nano Lett.* **17**, 7539 (2017).
 - ²⁰ X. Zhou, J. Cheng, Y. Zhou, T. Cao, H. Hong, Z. Liao, S. Wu, H. Peng, J. Xu, K. Liu, and D. Yu, *J. Am. Chem. Soc.* **137**, 7994-7997 (2015).
 - ²¹ L. M. Malard, T. V. Alencar, A. P. M. Barboza, K. F. Mak, and A. M. de Paula, *Phys. Rev. B* **87**, 201401 (2013).
 - ²² N. Kumar, S. Najmaei, Q. Cui, F. Ceballos, P. M. Ajayan, J. Lou, and H. Zhao, *Phys. Rev. B* **87**, 161403 (2013).
 - ²³ K.-I. Lin, Y.-H. Ho, S.-B. Liu, J.-J. Ciou, B.-T. Huang, C. Chen, H.-C. Chang, C.-L. Tu, and C.-H. Chen, *Nano Lett.* **18**, 793 (2018).
 - ²⁴ C. T. Le, D. J. Clark, F. Ullah, V. Senthilkumar, J. I. Jang, Y. Sim, M.-J. Seong, K.-H. Chung, H. Park, and Y. S. Kim, *Ann. Phys.* **528**, 551 (2016).
 - ²⁵ C. Janisch, Y. Wang, D. Ma, N. Mehta, A. L. Elías, N. Perea-López, M. Terrones, V. Crespi, and Z. Liu, *Sci. Rep.* **4**, 5530 (2014).
 - ²⁶ H. Zeng, G.-B. Liu, J. Dai, Y. Yan, B. Zhu, R. He, L. Xie, S. Xu, X. Chen, and W. Yao, *Sci. Rep.* **3**, 1608 (2013).
 - ²⁷ R. Wang, H.-C. Chien, J. Kumar, N. Kumar, H.-Y. Chiu, and H. Zhao, *ACS Appl. Mater. Interfaces* **6**, 314 (2013).
 - ²⁸ A. Säynätjoki, L. Karvonen, H. Rostami, A. Autere, S. Mehravar, A. Lombardo, R. Norwood, T. Hasan, N. Peyghambarian, H. Lipsanen, K. Kieu, A. Ferrari, M. Polini, and Z. Sun, *Nat. Comm.* **8**, 893 (2017).
 - ²⁹ R. I. Woodward, R. T. Murray, C. F. Phelan, R. E. P. de Oliveira, T. H. Runcorn, E. J. R. Kelleher, S. Li, E. C. de Oliveira, G. J. M. Fechine, G. Eda, and C. J. S. de Matos, *2D Mater.* **4**, 011006 (2017).
 - ³⁰ L. Karvonen, A. Säynätjoki, M. J. Huttunen, A. Autere, B. Amir-solaimani, S. Li, R. A. Norwood, N. Peyghambarian, H. Lipsanen, G. Eda, K. Kieu, and Z. Sun, *Nat. Comm.* **8**, 151714 (2017).
 - ³¹ H. Liu, Y. Li, Y. S. You, S. Ghimire, T. F. Heinz, and D. A. Reis, *Nat. Phys.* **13**, 262 (2017).
 - ³² M. Merano, *Opt. Lett.* **41**, 187 (2016).
 - ³³ D. J. Clark, C. T. Le, V. Senthilkumar, F. Ullah, H.-Y. Cho, Y. Sim, M.-J. Seong, K.-H. Chung, Y. S. Kim, and J. I. Jang, *Appl. Phys. Lett.* **107**, 131113 (2015).

- ³⁴ X. Miao, N. Xuan, Q. Liu, W. Wu, H. Liu, Z. Sun, and M. Ji, *ACS Appl. Mater. Interfaces* **9**, 34448-34455 (2017).
- ³⁵ C. Torres-Torres, N. Perea-López, A. L. Elías, H. R. Gutiérrez, D. A. Cullen, A. Berkdemir, F. López-Urías, H. Terrones, and M. Terrones, *2D Mater.* **3**, 021005 (2016).
- ³⁶ W. Wang, Y. Wu, Q. Wu, J. Hua, and J. Zhao, *Sci. Rep.* **6**, 22072 (2016).
- ³⁷ A. Castellanos-Gomez, M. Buscema, R. Molenaar, V. Singh, L. Janssen, H. S van der Zant, and G. A Steele, *2D Mater.* **1**, 011002 (2014).
- ³⁸ D. Li, H. Jussila, L. Karvonen, G. Ye, H. Lipsanen, X. Chen, and Z. Sun, *Sci. Rep.* **5**, 15899 (2015).
- ³⁹ “See supplemental material at [URL will be inserted by publisher] for more detailed description of the experimental methods, raman and photoluminescence characterization and technical details of the calculations”.
- ⁴⁰ H. Li, Q. Zhang, C. C. R. Yap, B. K. Tay, T. H. T. Edwin, A. Olivier, and D. Baillargeat, *Adv. Funct. Mater.* **22**, 1385–1390 (2012).
- ⁴¹ A. Berkdemir, H. R. Gutiérrez, A. R. Botello-Méndez, N. Perea-López, A. L. Elías, C.-I. Chia, B. Wang, V. H. Wang, F. López-Urías, J.-C. Charlier, H. Terrones, and M. Terrones, *Sci. Rep.* **3**, 01755 (2013).
- ⁴² H. J. Conley, B. Wang, J. I. Ziegler, R. F. Haglund Jr, S. T. Pantelides, and K. I. Bolotin, *Nano Lett.* **13**, 3626 (2013).
- ⁴³ M. Buscema, G. A. Steele, H. S. van der Zant, and A. Castellanos-Gomez, *Nano Research* **7**, 561 (2014).
- ⁴⁴ R. W. Boyd, *Nonlinear Optics* (Academic Press, New York, 2003).
- ⁴⁵ K. L. Seyler, J. R. Schaibley, P. Gong, P. Rivera, A. M. Jones, S. Wu, J. Yan, D. G. Mandrus, W. Yao, and X. Xu, *Nat. Nanotech.* **10**, 407-411 (2015).
- ⁴⁶ G. Wang, I. C. Gerber, L. Lagarde, A. Balocchi, M. Vidal, T. Amand, X. Marie, D. G. Mandrus, and B. Urbaszek, *2D Mater.* **2**, 045005 (2015).
- ⁴⁷ P. Tonndorf, R. Schmidt, P. Böttger, X. Zhang, J. Börner, A. Liebig, M. Albrecht, C. Kloc, O. Gordan, D. R. T. Zahn, S. M. de Vasconcellos, and R. Bratschitsch, *Opt. Express* **21**, 4908 (2013).
- ⁴⁸ J. Qian, Z. Zhu, A. Qin, W. Qin, L. Chu, F. Cai, H. Zhang, Q. Wu, R. Hu, B. Z. Tang, and S. He, *Adv. Mater.* **27**, 2332 (2015).
- ⁴⁹ Z. Ye, T. Cao, K. O'Brien, H. Zhu, X. Yin, Y. Wang, S. G. Louie, and X. Zhang, *Nature* **513**, 11 (2014).
- ⁵⁰ K. He, N. Kumar, L. Zhao, Z. Wang, K. F. Mak, H. Zhao, and J. Shan, *Phys. Rev. Lett.* **113**, 026803 (2014).
- ⁵¹ Q. Liu, B. Guo, Z. Rao, B. Zhang, and J. R. Gong, *Nano Lett.* **13**, 2436 (2013).
- ⁵² W. Dai, H. Dong, B. Fugetsu, Y. Cao, H. Lu, X. Ma, and X. Zhang, *Small* **11**, 4158 (2015).
- ⁵³ J. H. Yu, S.-H. Kwon, Z. Petrusek, O. K. Park, S. W. Jun, K. Shin, M. Choi, Y. I. Park, K. Park, H. B. Na, N. Lee, D. W. Lee, J. H. Kim, P. Schwill, and T. Hyeon, *Nat. Mater.* **12**, 359 (2013).
- ⁵⁴ C. T. Le, D. J. Clark, F. Ullah, J. I. Jang, V. Senthilkumar, Y. Sim, M.-J. Seong, K.-H. Chung, J. W. Kim, S. Park, S. H. Rhim, G. Kim, and Y. S. Kim, *ACS Photonics* **4**, 38 (2017).
- ⁵⁵ D. Clark, V. Senthilkumar, C. Le, D. Weerawarne, B. Shim, J. Jang, J. Shim, J. Cho, Y. Sim, M.-J. Seong, S. H. Rhim, A. J. Freeman, K.-H. Chung, and Y. S. Kim, *Phys. Rev. B* **90**, 121409 (2014).
- ⁵⁶ G.-B. Liu, W.-Y. Shan, Y. Yao, W. Yao, and D. Xiao, *Physical Review B* **88**, 085433 (2013).
- ⁵⁷ A. Marini, C. Hogan, M. Grunig, and D. Varsano, *Comp. Phys. Comm.* **180**, 1392 (2009).